B. Medley[1], J. T. M. Lenaerts[2], M. Dattler[1,3], E. Keenan[2], and N. Wever[2]

[1]Cryospheric Sciences Laboratory, NASA Goddard Space Flight Center, Greenbelt, MD, USA.

[2]Department of Atmospheric and Oceanic Sciences, University of Colorado Boulder, Boulder, CO, USA.

[3]Department of Atmospheric and Oceanic Science, University of Maryland College Park, College Park, MD, USA.

Corresponding author: Brooke Medley (brooke.c.medley@nasa.gov)

Key Points:

- We predict snow accumulation spatial deviations through synthesis of topographic and atmospheric characteristics on a 1-km grid
- Redistribution processes likely reduce Antarctic surface mass balance between 43.0 Gt yr^{-1} and 109.3 Gt yr^{-1}
- We link seasonal anomalies in snow accumulation to the relationship between spatial accumulation variability and height change.

Abstract

Sub-grid-scale processes occurring at or near the surface of an ice sheet have a potentially large impact on local and inetegrated surface mass balance (SMB) via redistribution and sublimation. Given observational complexity, they are either ignored or parametereized over large-length scales. Here, we train random forest models to predict 1-km variability in snow accumulation rates over the Antarctic Ice Sheet using atmospheric variables and topographic characteristics. Observations of snow accumulation from both *in situ* and airborne radar data provide the predictors needed to train the random forest models. We find that sub-grid-scale processes yield a net reduction in grounded SMB of ~50 Gt yr^{-1}, and our model evaluation suggests this is likely a lower bound. Spatial correlation between the predicted snow accumulation variability with satellite-derived surface height change indicates that sub-grid-scale processes operate differently through time, in tandem with temporal snow accumulation anomalies.

1 Introduction

Large-scale snowfall events deposit a substantial amount of freshwater over the Antarctic Ice Sheet (AIS), acting in opposition to present-day sea-level rise. Approximately 7 mm of global sea-level equivalent falls annually in the form of snow over the entire ice sheet (Mottram et al., 2021); any short-to-long-term deviations in time and space from this mean will directly impact the temporal evolution mass balance of the AIS and its individual glacial drainage systems (Rignot et al., 2019; Smith et al., 2020). State-of-the-art atmospheric models do not agree, however, on the total magnitude of annual snow accumulation (Mottram et al., 2021), ranging by more 500 Gt yr^{-1}, a value which largely overshadows a reconciled AIS total mass balance of -109 Gt yr^{-1} (Shepherd et al.,

2018). This lack of constraint yields arguably the largest source of uncertainty in estimates of AIS mass balance and its contribution to global sea level (Rignot et al., 2019; Shepherd et al., 2018; Smith et al., 2020). We aim to constrain the magnitude of snow accumulation over the AIS at fine spatial resolution within a global atmospheric model using airborne and ground-based measurements of snow accumulation.

While snowfall events over the ice sheet are synoptic, blowing snow processes occurring prior to or after deposition at the surface impart local-scale variability as snow is redistributed or preferentially sublimated (Lenaerts et al., 2019). At present, global atmospheric models are not capable of accounting for these small-scale impacts (Gelaro et al., 2017), and only a small handful of regional climate models simulate these processes albeit at much coarser scales than they actually occur (Agosta et al., 2019; Van Wessem et al., 2018). A lack of observed accumulation rates at the scale necessary to measure these local processes challenged development of both physics-based and empirical models. Recently, ground-based (Das et al., 2013; Spikes et al., 2004) and airborne (Dattler et al., 2019b; Medley et al., 2013) radar observations of the ice sheet's near-surface internal stratigraphy have revealed the small-scale variability in snow accumulation at fine along-track resolution and over large swaths of the ice sheet. Here, we built on prior work (Das et al., 2013; Dattler et al., 2019b; Scambos et al., 2012; Studinger et al., 2020) investigating small-scale variability in snow accumulation and regions of net scour, including their relationship to local topography and wind characteristics, to predict small-scale deposition and erosion of snowfall at the ice-sheet scale.

The mean annual surface mass balance ($\pm$ 1 standard deviation) derived from NASA's Modern-Era Retrospective analysis for Research and Applications, Version 2 (MERRA-2; Gelaro et al., 2017) over the AIS totals to 2797 $\pm$ 159 Gt yr^{-1}, with 2185 $\pm$ 133 Gt yr^{-1} over grounded ice and 612 $\pm$ 39 Gt yr^{-1} over floating ice. This global model is coarsely resolved and does not include physical processes that occur over ice sheets over short length scales, such as blowing snow. Regional climate models (RCMs) (Agosta et al., 2019; Lenaerts et al., 2012; Van Wessem et al., 2018) have accounted for these processes with varying degrees of complexity; however, the parameterizations hold for transport over large length scales (several 10s of km), limiting their applications within finer-scale studies. For instance, results from a 5 km RCM run over West Antarctica did not show significant improvement in SMB representation against the same RCM run at 27 km (Lenaerts et al., 2018). Nevertheless, the snow transport from these two RCMs suggest regions of mass gain (deposition) and loss (erosion) and yet the net impact on mass balance is on the order of a few Gt yr^{-1} (Agosta et al., 2019). Another study (Das et al., 2013) used thresholding of wind and topographic regimes to determine regions of net wind scour (i.e., SMB < 0) which yielded an estimated loss of snow mass input due to wind erosion between 11 and 36.5 Gt yr^{-1}. The latter study does not provide context for the total impact of snow redistribution because net snow deposition was not considered, providing only one side of the balance equation. Here, we built a static map of

snow deposition and erosion over the grounded and floating portions of the AIS at 1-km resolution.

2 Data

2.1 ICESat-2 Surface Height and Height Change

Launched in 2018, NASA's next generation Ice, Cloud, and land Elevation satellite (ICESat-2) is a photon-counting laser altimeter designed to provide precise, repeateable measurements of ice-surface height change every 91 days, globally to latitudes not exceeding 88° in magnitude (Markus et al., 2017). Here, we use the ICESat-2 L3A Land Ice Height, Version 2 (ATL06; Smith et al. (2019)) collected during the first three 91-day cycles (October 14, 2018–June 26, 2019). Because ICESat-2 was not pointing at its designed repeat tracks during the first two cycles, data collected during the first ~180 days provide additional height measurements, which improved spatial coverage. More details regarding building a DEM using ICESat-2 data are in Section S2.

To investigate spatial patterns of height change, we also use the ICESat-2 L3B Slope-Corrected Land Ice Height Time Series, Version 4 (ATL11; Smith et al. (2021)) spanning cycles 3–11 (March 29, 2019–June 23, 2021). The ATL11 dataset provides along-track height that is slope-corrected onto a reference pair track for each cycle beginning with cycle 3 when ICESat-2 began pointing at its designed reference ground tracks. We eliminate less robust surface heights by using heights that have a quality summary flag set to zero.

2.2 Atmospheric

We use several atmospheric variables from NASA's Modern-Era Retrospective analysis for Research and Applications, Version 2 (MERRA-2; Gelaro et al., 2017), including hourly 10-m winds, and snowfall in addition to monthly evaporation, humidity, and surface temperature from January 1, 1980 to December 31, 2019 (GMAO, 2015a, 2015b, 2015c, 2015d). MERRA-2 data are provided globally at 0.5° latitude by 0.625° longitude resolution.

2.3 Snow Accumulation

2.3.1 Snow Radar

Snow accumulation measurements over the large scales of interest to this work are few in number. Interpretation of the near surface firn stratigraphy from NASA's Operation IceBridge (OIB) snow radar data by Dattler et al. (2019b) provides a comprehensive analysis of variable snow accumulation rates at 100 m along-track spacing over large portions of the Antarctic Peninsula and West Antarctica and portions of East Antarctica (Figure S1). The data were collected between 2010 and 2017; however, because of the largely unvarying stratigraphic deviations with depth, the Dattler et al. (2019b) dataset provides robust deviations in the snow accumulation rate from the large-scale mean. These data are hereinafter referred to as OIB accumulation rates (Dattler et al., 2019a).

We also derive snow accumulation rates (Section 4.2.1) from additional snow radar data collected October 25, 2019 (Leuschen, 2014) that was released subsequent to the development of the Dattler et al. (2019b) dataset. We replicate the methodology from Dattler et al. (2019b).

2.3.2 SurfAce Mass Balance of Antarctica (SAMBA)

To supplement the airborne OIB measurements, we also use the SurfAce Mass Balance of Antarctica (SAMBA) dataset (Figure S1), which provides ground-based measurements of snow accumulation covering a wide-range of locations and time periods (Favier et al., 2013). For this work, we use only the data of highest quality ("A" rated).

3 Prediction of Snow Redistribution

We built a 1-km static map of predicted anomalies in snow accumulation from the background large-scale MERRA-2 annual mean value using airborne and ground-based observations of snow accumulation and a series of topographic and atmospheric predictors. We next outline the various predictors, and then explain the random forest method implemented for prediction.

3.1 Predictors

In all, we used 11 predictors that described the topographic and climatic characteristics as well as their interactions over the AIS. Topographic predictors were based on the DEM described in Section S2 and include: height, slope, aspect, curvature, and a 20 km high-pass filter of the surface height (Figures S2-S6). Prior to determination of the topographic characteristics, we applied a 6-km low-pass filter to the DEM to minimize any tracking artifacts. Climatic predictors were built from MERRA-2 mean annual variables and include: 10-meter wind speed, 10-meter wind direction, air temperature, specific humidity, total precipitation-minus-evaporation ($P-E$; Figures S7-S11). Finally, we use the mean slope in the mean wind direction (Figure S12), the dot product of the wind and slope vectors, as described in the Section S3.

3.2 Training Data

The OIB and SAMBA snow accumulation datasets were modified to represent the relative deviation in snow accumulation from the large-scale MERRA-2 mean annual $P-E$ (i.e., the percent deviation from MERRA-2). Each dataset was then gridded onto the same 1-km grid as the DEM by averaging points that fall within the same grid cell. The number of points used within a given grid cell was stored for weighting purposes. As done with the DEM, we applied a 6-km low-pass filter to the OIB gridded accumulation rates; however, because the SAMBA grid is discontinuous, we did not apply a filter.

3.3 Random Forest Method

Using the random forest (RF) regression algorithm we predicted the magnitude of snow redistribution over the entire AIS using 11 predictors (Section 3.1) and 2 training datasets (Section 3.2). The OIB (n = 17,593) and SAMBA (n =

2,969) gridded data were randomly sampled into 80% training and 20% testing partitions. Thus, a total of 16,451 observations are used to train the ensemble of decision trees. The testing partition was not used to build the RF model but rather for performance evaluation. Specifically, we employed bootstrap aggregation method (i.e., bagging) and an interaction-based predictor-selection technique for all RF experiments to increase detection of predictor interactions (Loh, 2002). The ensemble bagging technique builds decision trees each generated from a random sample with replacement of the training dataset, diversifying the individual trees. The training data were weighted by the number of OIB or SAMBA observations that were used in determining the grid cell average (Section 3.2).

Using two RF parameter scenarios (optimized and standard practice; see Section S4), we built two final RF of 1,000 decision trees for prediction of snow redistribution using our ICESat-2 DEM. The standard deviation of predictions amongst the individual trees provided an assessment of the quality of final prediction. To investigate the impact of the choice of surface height model, we employed the same exercise outlined above using the REMA DEM resampled to the same 1-km grid as our ICESat-2 DEM. Two CryoSat-2 DEMs were not used (see Sections S1.2 and S2.1). Thus, we built 4 models of snow redistribution.

4 Results

4.1 Snow Redistribution Predictions

Typical relative deviations (Figure 1a) from the large-scale MERRA-2 mean accumulation rate range between -29.8% to +17.4% (lower and upper 5%), whereas absolute deviations (Figure 1b) span -48.0 to +28.2 mm w.e. yr^{-1}. Similarly, the uncertainties in the relative deviations (Figure 1c) range between 9.4% and 38.8%, whereas the absolute uncertainties (Figure 1d) span 4.4 to 130.7 mm w.e. yr^{-1}. Integrated over the entire ice sheet, the RF models yield similar impacts on Antarctic-wide SMB. Specifically, they predict a reduction in net SMB between -33.3 Gt yr^{-1} and -49.7 Gt yr^{-1} (Table S2). The SMB impact on ice shelves is relatively low as the predictions suggest a minimally more positive SMB (+2.6 to +5.7 Gt yr^{-1}). All RF models indicate large reductions in SMB over grounded ice (-39.0 to -53.5 Gt yr^{-1}).

Uncertanty calculations for the integrated values account for correlated errors within a 20-km radius, a value chosen to correspond with the 20-km high-pass filtered surface heights used as a predictor. Because no single RF model outperformed the others (Table S2), we present the most likely representation of snow accumulation deviations as the mean of all four predictions; we conservatively combine their uncertainties assuming they are perfectly correlated (i.e., root sum of squares). This yields integrated SMB deviations for floating and grounded ice of $+4.4 \pm 8.1$ Gt yr^{-1} and -47.3 ± 18.1 Gt yr^{-1}. Hereinafter, all results presented are in reference to this scenario.

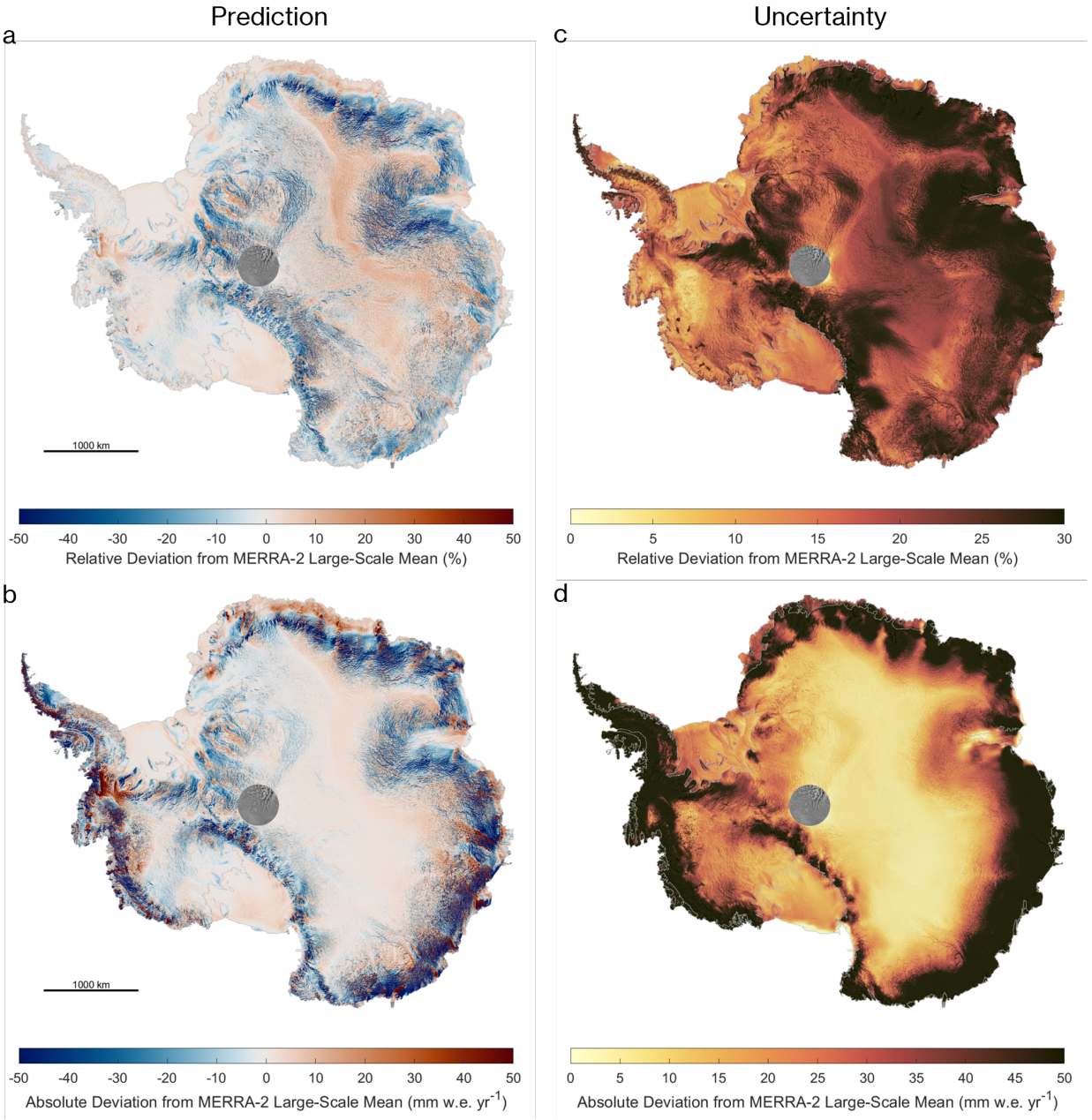

Figure 1. Predicted deviations in the snow accumulation rate from the large-scale mean and their uncertainty. The relative (a) and absolute (b) predicted deviations in snow accumulation show heterogenous patterns of deposition/erosion that vary by region. The uncertainty in both relative (c) and absolute (d) predictions are the largest for the coastal slopes of the East Antarctic Ice Sheet.

4.2 Comparison with ICESat-2 Height Change

4.2.1 Case Study with Coincident OIB Snow Radar

Over long timescales and an unchanging climate, the amount of snow that falls and accumulates is balanced by firn compaction and the loss of firn via conversion to ice suggesting that ice-surface-height does not evolve as a result of snowfall processes; however, at short subannual lengthscales, episodic and seasonal evolution of precipitation and temperature at the surface have a large impact on surface-height changes. Thus, if the static model of snow redistribution that we have generated is stable in time, then we should observe height changes that resemble the variability in snow accumulation rates. To investigate the importance of this variability on our interpretation of ice-surface-height evolution, we analyze the relationship between ICESat-2 observed changes in the ice surface with our snow redistribution model, OIB snow radar data, and MERRA-2 climate.

In 2019, OIB underflew ICESat-2 ground tracks over coastal Wilkes and Victoria Land, which provides us the ability to directly compare OIB snow radar, our snow redistribution models, and ICESat-2 height change. We analyze a 100-km segment from October 25, 2019 that follows a trajectory near-perpendicular to the coast, transiting to higher elevations (Figure 2). The ICESat-2 height change along this ground track between May 2, 2020 and August 1, 2020 shows an overall increase in height with significant small-scale variations along track (Figure 2a). We next compare the ICESat-2 data with coincident OIB snow radar data by following the same procedure as outlined by Dattler et al. (2019b) to produce accumulation rates across the entire segment after tracking a single snow radar horizon through space. We show the resulting radar-derived accumulation rates, the snow redistribution models from this work, and the MERRA-2 mean $P-E$ interpolated to each radar measurement in Figure 2b, and the snow radar echogram and tracked layer in Figure 2c. As with the Dattler et al. (2019b) dataset, our radar-derived accumulation rates were calculated in a way that matches them with the large-scale MERRA-2 mean. That assumption does not impact our assessment of the small-scale variability in the snow accumulation.

Based on this exercise, we confirm that our snow redistribution models are capable of reproducing small-scale variations in the snow accumulation rate and that there are not substantial differences between the RF models. We note that these snow radar data were collected in 2019 and are not part of the OIB accumulation dataset compiled by Dattler et al. (2019b), which used data collected up through 2017. Thus, the comparison here is independent of our RF model development. We also confirm that the RF models underestimate the total magnitude of the deviations. Nevertheless, we observe significant correlation between the radar-derived accumulation rates, RF models of snow accumulation, and ICESat-2 height change variability.

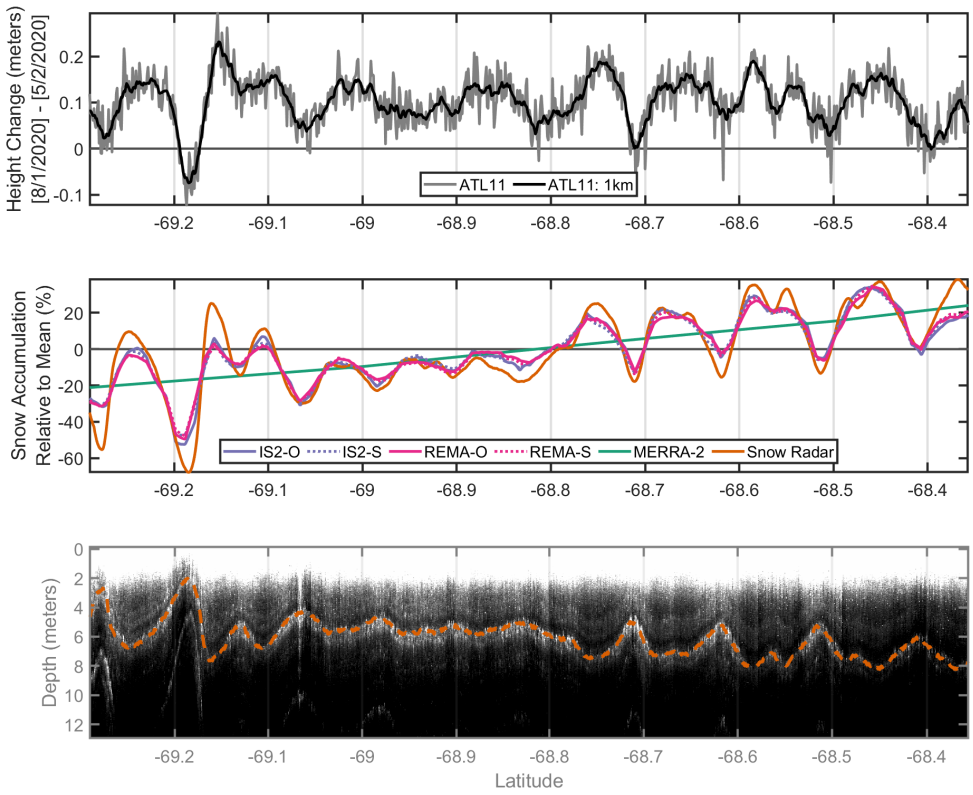

Figure 2. Comparison of ICESat-2 ATL11 height change with the random forest models of snow accumulation variability and OIB radar-derived snow accumulation rates. (a) The wintertime change in height (May 2, 2020–August 1, 2020) over a 100-km ICESat-2 ground track posted at 60 m (grey) and with a 1-km moving average applied (black). (b) Snow accumulation rates relative to the large-scale mean from MERRA-2 (green), the four random forest snow accumulation models (pink/purple) named by the DEM used and whether the model used optimized (O) or standard (S) practice parameters, and coincident OIB snow radar-derived snow accumulation rates. (c) OIB snow radar echogram collected October 25, 2019 that is coincident in space with the ICESat-2 ATL11 reference pair track 2. The layer traced in dashed orange provided the basis of the radar-derived snow accumulation rates represented by an orange line in (b).

4.3 Ice-Sheet-Wide Height Change and Snow Accumulation Variability

ICESat-2 ATL11 provides along-track, slope-corrected heights spanning nine 91-day cycles, providing seasonal height change over a two-year period. For each reference pair track, we calculate cycle-by-cycle height change (i.e., height

change over a 91-day interval) and apply a 6-km moving mean to match the same filter applied to our ICESat-2 DEM (Section S2). For each reference pair track, we find the mean MERRA-2 $P-E$ anomaly over the exact time epoch for each cycle and for that specific track. This step provides the temporal accumulation rate anomaly along each reference pair track over the same time and space as the ICESat-2 ATL11 data. We also interpolate our static RF snow redistribution models onto the same along-track ATL11 heights. To investigate the relationship between observed height change and our predicted deviations in snow accumulation, we correlate the the ATL11 height changes with our mean RF model of snow variability along 50-km segments for each cycle pair. This relationship, as well as the temporal accumulation anomaly over each cycle pair, is summarized in Figure 3. We find that the sign and magnitude of the correspondence between spatial variations in snow accumulation and observed height changes varies by season.

5 Discussion

We use a novel combination of snow accumulation rates derived from OIB shallow radar data, as well as other observational constraints, with topographic and atmospheric characteristics derived from ICESat-2 surface height data and MERRA-2 to predict snow accumulation rates on a 1-km grid. Neither selection of the RF model parameters nor choice of DEM largely impacted the results, suggesting that we used a robust choice of predictors and that the models likely do not suffer from overfitting the training data. Not all predictors, however, were equally important. We found in order that aspect, wind speed, curvature, wind direction, and 20 km high-pass filter of the surface height were the most influential predictors. The importance of wind speed and curvature is in line with prior studies, which used them as the sole predictors of snow transport (Agosta et al., 2019). In addition, directional information is relevant considering aspect and wind direction played a key role in the predictions.

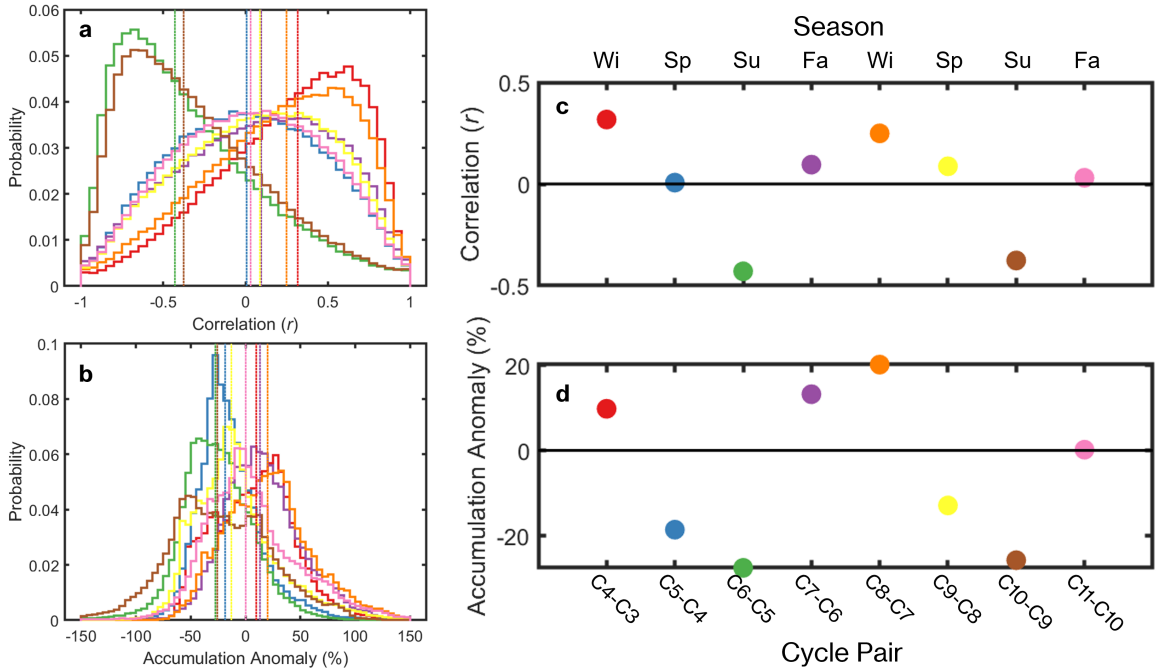

Figure 3. Comparison of 50-km along-track (a) correlations between the mean random forest snow accumulation model and ICESat-2 ATL11 height change for 8 cycle pairs and (b) temporal snow accumulation rate anomalies over the entire AIS. The results are presented as histograms of either the correlation coefficient or the magnitude of the temporal anomaly in snow accumulation over 50-km ATL11 segments and are color coded by cycle pair. The median of each distribution is displayed as a dotted vertical line. (c) The median histogram correlation coefficient values from (a) plotted in time referenced to the cycle pair and its associated season. (d) the same as (c) but a time series of the median accumulation anomaly. Colors in both (c) and (d) match those from (a) and (b).

Our new predictions of snow redistribution over the entire AIS suggest an additional, unaccounted for mass loss (± 1 uncertainty) of 44.3 ± 20.2 Gt yr^{-1}, which is split into a loss of 48.1 ± 18.1 Gt yr^{-1} over grounded ice and a minor gain of 3.8 ± 8.1 Gt yr^{-1} over floating ice. We find that while our predictive model is highly capable of reproducing the spatial variability (or sign) in snow redistribution, it consistently *underestimates the magnitude* of that variability. Thus, we expect our predictions reference a lower bound on AIS mass loss due to snow redistribution processes. Evaluation of model performance indicates that this underestimation is likely between 50 and 60%, suggesting that the relevance of snow redistribution processes for AIS mass balance could more than double, approaching net loss in exceedance of 100 Gt yr^{-1}; however, more observations

are required to confirm this interpretation. Atmospheric modelling work using regional atmospheric climate model RACMO2 found the drifting snow sublimation and erosion accounted for a net loss of 107 Gt yr^{-1} over the entire AIS (Van Wessem et al., 2018), a number which falls within our our expected bounds when accounting for the model underestimation (87 - 109 Gt yr^{-1}).

From an integrated mass balance perspective, the majority of that mass loss occurs across the East Antarctic Ice Sheet (EAIS; 43.8 Gt yr^{-1}) followed by the West Antarctic Ice Sheet (WAIS; 4.5 Gt yr^{-1}) and the Antarctic Peninsula (AP; -0.2 Gt yr^{-1}). Because there are quite a number of measurements from West Antarctica, the uncertainties in both and absolute and relative sense are quite low. Thus, any additional measurements from WAIS will likely not provide much improvement to our predictions. Interestingly, traverse measurements do exist within the sector spanning eastern Dronning Maud Land to the Amery Ice Shelf; however, the uncertainties here remain large, which could be a function of the very large snow redistribution processes and perhaps a strongly different climate and/or topography as the region contributing the most measurements (i.e., WAIS).

5.1 Snow accumulation variability and height change

At seasonal time scales, variations in surface height fluctuate in response to strong positive or negative snowfall anomalies in time, albeit in a different fashion. Over the entire AIS, an integrated positive anomaly (Figure 3: red/orange) typically occurs in winter, when the correlation between our snow accumulation model is positively correlated with observed height changes. Locations that receive anomalously higher snow accumulation than its immediate vicinity due to redistribution experience larger height increases (i.e., receive more snowfall), which have not yet been modulated by their enhanced compaction rates, which operate on slower timescales. The opposite is true in the summer when the ice sheet typically experiences negative snowfall anomalies (Figure 3: green/brown): locations that receive anomalously higher snow accumulation than its immediate vicinity due to redistribution experience larger height decreases. Even though a region might not receive any snow accumulation, densification processes are more rapid where the long-term snow accumulation rate is larger; thus, under anomalously low snowfall conditions, we observe the spatial variations in compaction rates that are generated from the spatial variations in the long-term accumulation rate.

The signal when integrated over the entire ice sheet is less obvious in spring and summer. We hypothesize that while during spring (Figure 3: blue/yellow) there are typically large negative anomalies in snow accumulation, the firn column remains cold coming out of winter (i.e., a thermal lag), which reduces compaction rates and thus the correspondence between the local snow accumulation rate anomalies and ATL11 height changes. We expect the opposite as well: during the fall (Figure 3: purple/pink), the firn column is warmer leading to more compaction, which modulates the typical positive snow accumulation anomalies, although the signal is weaker.

These results indicate that substantial deviations in ATL11 height changes along-track exist in response to spatial variations in the long-term accumulation rate due to local-scale processes (i.e., redistribution/sublimation) and that the sign of the height change anomaly likely reflects the sign of the temporal accumulation anomaly over the cycle-pair epoch. Thus, small-scale variability observed in ATL11 derived height change reflect surface processes and should not be considered instrument noise but rather highlight precision and data product capability. Thus, any studies interested in small-scale changes will need to strongly consider the impact of surface processes on the interpretation of the observed spatiotemporal height changes.

5.2 Limitations

While we have provided a product of AIS sub-grid-scale snow accumulation that is largely capable of reproducing its spatial variability, several limitations remain that if addressed could improve the methodology. In the generation of the DEM, we chose to remove any ATL06 surface heights that had an RMS error larger than 0.1 m, which likely excluded too much data in steeply sloping regions. This limitation could be overcome using an RMS threshold as a function of slope. Because the technique used to derive the OIB snow accumulation rates is tied to the MERRA-2 large-scale mean (Dattler et al., 2019b), we only use MERRA-2 atmospheric data as predictors. Future work replicating Dattler et al. (2019b) using other atmospheric models would allow for predictions with other atmospheric models.

Other limitations stem from the predictor and predictand training data used. While the topographic data are well resolved at 1-km resolution, the atmospheric data only resolves variables at several 10s of km; thus, atmospheric downscaling could lead to improved predictions. The set of predictors used might also be incomplete. Our analysis suggests that height change from ICESat-2 is also strongly related to the small-scale variability in snow accumulation rates, and it could provide more constraint in the future at the ice-sheet-wide scale. Similarly, the RF model relies on training data spanning several different atmospheric and topographic regimes, however, most of the OIB accumulation rates are from the Antarctic Peninsula and West Antarctica. The SAMBA dataset fills in much of the missing areas in East Antarctica, but much of the data are representative of a single point, which might not be representative of the 1 km-by-1 km region in which it falls. Our weighting scheme likely minimized the impact, but it will never be entirely overcome until we have more measurements of snow accumulation over large areas.

6 Conclusions

While atmospheric models generally agree on the spatial signatures of snow accumulation over the AIS (Mottram et al., 2021), they at present either do not account for drifting snow processes or do so at a coarse scale. Shallow radar studies have revealed significant deviations in the snow accumulation rate at sub-grid-cell scales (Medley et al., 2013; Richardson et al., 1997; Spikes et al.,

2004), which suggest that atmospheric model evaluations against sparse point measurements of snow accumulation are likely flawed. The predictions generated for this study will hopefully provide new context for model evaluations by eliminating some of the scale ambiguity in model-observation comparisons. The results also suggest that redistribution processes at the surface remain a large unknown when estimating the ice sheet surface mass balance. The resulting spatial anomalies in the net snow accumulation rate are manifested in satellite-derived measurements of surface height changes, which also adds uncertainty to interpretation especially when considering seasonal timescales. Additional measurements of the small-scale variations in the snow accumulation rate as well as more targeted studies bringing together satellite altimetric height changes and firn densification models at the local scale would prove more edifying in untangling the full response of the surface to these various processes.

Acknowledgments

The work was supported by NASA Cryopsheric Sciences and the NASA Interdisciplinary Research in Earth Sciences programs.

Open Science

The ICESat-2 data used in this study are available in Smith et al. (2019) and Smith et al. (2021). The MERRA-2 data used are in GMAO (2015a, 2015b, 2015c, 2015d). The IceBridge snow accumulation rates are available in Dattler et al. (2019a). The IceBridge snow radar data are available in Leuschen et al. (2014), and the IceBridge Airborne Topographic Mapper data are available in Krabill et al. (2014). The Reference Elevation Model of Antarctica is available in Howat et al. (2019), and the CryoSat-2 DEMs are available in Helm et al. (2014a, 2014b) and Slater et al. (2018). The SAMBA data (Favier et al., 2013) are available at http://pp.ige-grenoble.fr/pageperso/faviervi/database.php. The data created in this study are available temporarily during review via this link: https://nasagov.box.com/shared/static/4ywga918q7akxba4gmgk9ifejflo0yze.zip. Once accepted, the data will be made available in an open access repository.

References

Agosta, C., Amory, C., Kittel, C., Orsi, A., Favier, V., Gallée, H., et al. (2019). Estimation of the Antarctic surface mass balance using the regional climate model MAR (1979-2015) and identification of dominant processes. *Cryosphere*, *13*(1), 281–296.Das, I., Bell, R. E., Scambos, T. A., Wolovick, M., Creyts, T. T., Studinger, M., et al. (2013). Influence of persistent wind scour on the surface mass balance of Antarctica. *Nature Geoscience*, *6*(5), 367–371.Dattler, M. E., Lenaerts, J. T. M., & Medley, B. (2019a). Antarctic Snow Radar-Derived Relative Accumulation Product [Data set]. Zenodo. https://doi.org/10.5281/zenodo.3534315Dattler, M. E., Lenaerts, J. T. M., & Medley, B. (2019b). Significant Spatial Variability in Radar-Derived West Antarctic Accumulation Linked to Surface Winds and Topography. *Geophysical Research Letters*, *46*(22), 13126–13134.Favier, V., Agosta, C.,

Parouty, S., Durand, G., Delaygue, G., Gallée, H., et al. (2013). An updated and quality controlled surface mass balance dataset for Antarctica. *The Cryosphere*, *7*(2), 583–597.Gelaro, R., McCarty, W., Suárez, M. J., Todling, R., Molod, A., Takacs, L., et al. (2017). The modern-era retrospective analysis for research and applications, version 2 (MERRA-2). *Journal of Climate*, *30*(14), 5419–5454.GMAO (2015a). MERRA-2 tavg1_2d_flx_Nx: 2d,1-Hourly,Time-Averaged,Single-Level,Assimilation,Surface Flux Diagnostics V5.12.4 [Data set]. NASA Goddard Earth Sciences Data and Information Services Center. https://doi.org/10.5067/7MCPBJ41Y0K6GMAO (2015b). MERRA-2 tavg1_2d_slv_Nx: 2d,1-Hourly,Time-Averaged,Single-Level,Assimilation,Single-Level Diagnostics V5.12.4 [Data set]. NASA Goddard Earth Sciences Data and Information Services Center. https://doi.org/10.5067/VJAFPLI1CSIVGMAO (2015c). MERRA-2 tavgM_2d_flx_Nx: 2d,Monthly mean,Time-Averaged,Single-Level,Assimilation,Surface Flux Diagnostics V5.12.4 [Data set]. NASA Goddard Earth Sciences Data and Information Services Center. https://doi.org/10.5067/0JRLVL8YV2Y4GMAO (2015d). MERRA-2 tavgM_2d_slv_Nx: 2d,Monthly mean,Time-Averaged,Single-Level,Assimilation,Single-Level Diagnostics V5.12.4 [Data set]. NASA Goddard Earth Sciences Data and Information Services Center. https://doi.org/10.5067/AP1B0BA5PD2KHelm, V., Humbert, A., & Miller, H. (2014a). Elevation and elevation change of Greenland and Antarctica derived from CryoSat-2. *The Cryosphere*, *8*(4), 1539–1559.Helm, V., Humbert, A., & Miller, H. (2014b). Elevation Model of Antarctica derived from CryoSat-2 in the period 2011 to 2013, links to DEM and uncertainty map as GeoTIFF [Data set]. *In supplement to: Helm, V et al. (2014): Elevation and elevation change of Greenland and Antarctica derived from CryoSat-2. The Cryosphere, 8(4), 1539-1559, https://doi.org/10.5194/tc-8-1539-2014*. PANGAEA. https://doi.org/10.1594/PANGAEA.831392Howat, I. M., Porter, C., Smith, B. E., Noh, M.-J., & Morin, P. (2019). The Reference Elevation Model of Antarctica. *The Cryosphere*, *13*(2), 665–674. https://doi.org/10.5194/tc-13-665-2019Krabill, W. (2014). IceBridge ATM L2 Icessn Elevation, Slope, and Roughness, Version 2 [Data set]. NASA National Snow and Ice Data Center DAAC. https://doi.org/10.5067/CPRXXK3F39RVLenaerts, J. T., Van den Broeke, M. R., Van de Berg, W. J., Van Meijgaard, E., & Kuipers Munneke, P. (2012). A new, high-resolution surface mass balance map of Antarctica (1979–2010) based on regional atmospheric climate modeling. *Geophysical Research Letters*, *39*(4).Lenaerts, J. T., Ligtenberg, S. R., Medley, B., Van de Berg, W. J., Konrad, H., Nicolas, J. P., et al. (2018). Climate and surface mass balance of coastal West Antarctica resolved by regional climate modelling. *Annals of Glaciology*, *59*(76pt1), 29–41.Lenaerts, J. T., Medley, B., van den Broeke, M. R., & Wouters, B. (2019). Observing and modeling ice sheet surface mass balance. *Reviews of Geophysics*, *57*(2), 376–420.Leuschen, C. (2014). IceBridge Snow Radar L1B Geolocated Radar Echo Strength Profiles, Version 2 [Data set]. NASA National Snow and Ice Data Center DAAC. https://doi.org/10.5067/FAZTWP500V70Loh, W.-Y. (2002). Regression tress with unbiased variable selection and interaction detection. *Statistica Sinica*, 361–386.Markus, T., Neumann, T., Martino, A., Abdalati, W., Brunt, K.,

Csatho, B., et al. (2017). The Ice, Cloud, and land Elevation Satellite-2 (ICESat-2): science requirements, concept, and implementation. *Remote Sensing of Environment*, *190*, 260–273.Medley, B., Joughin, I., Das, S. B., Steig, E. J., Conway, H., Gogineni, S., et al. (2013). Airborne-radar and ice-core observations of annual snow accumulation over Thwaites Glacier, West Antarctica confirm the spatiotemporal variability of global and regional atmospheric models. *Geophysical Research Letters*, *40*(14), 3649–3654.Mottram, R., Hansen, N., Kittel, C., van Wessem, J. M., Agosta, C., Amory, C., et al. (2021). What is the surface mass balance of Antarctica? An intercomparison of regional climate model estimates. *The Cryosphere*, *15*(8), 3751–3784.Richardson, C., Aarholt, E., Hamran, S.-E., Holmlund, P., & Isaksson, E. (1997). Spatial distribution of snow in western Dronning Maud Land, East Antarctica, mapped by a ground-based snow radar. *Journal of Geophysical Research: Solid Earth*, *102*(B9), 20343–20353.Rignot, E., Mouginot, J., Scheuchl, B., Van Den Broeke, M., Van Wessem, M. J., & Morlighem, M. (2019). Four decades of Antarctic Ice Sheet mass balance from 1979–2017. *Proceedings of the National Academy of Sciences*, *116*(4), 1095–1103.Scambos, T. A., Frezzotti, M., Haran, T., Bohlander, J., Lenaerts, J. T. M., Van Den Broeke, M. R., et al. (2012). Extent of low-accumulation'wind glaze'areas on the East Antarctic plateau: implications for continental ice mass balance. *Journal of Glaciology*, *58*(210), 633–647.Shepherd, A., Ivins, E., Rignot, E., Smith, B., Van Den Broeke, M., Velicogna, I., et al. (2018). Mass balance of the Antarctic Ice Sheet from 1992 to 2017. *Nature*, *558*, 219–222.Slater, T., Shepherd, A., McMillan, M., Muir, A., Gilbert, L., Hogg, A. E., et al. (2018). A new digital elevation model of Antarctica derived from CryoSat-2 altimetry. *Cryosphere*, *12*(4), 1551–1562.Smith, B., Fricker, H. A., Gardner, A., Siegfried, M. R., Adusumilli, S., Csath??, B. M., et al. (2019). ATLAS/ICESat-2 L3A Land Ice Height, version 2 [Data set]. NASA National Snow and Ice Data Center DAAC. https://doi.org/10.5067/ATLAS/ATL06.002Smith, B., Fricker, H. A., Gardner, A. S., Medley, B., Nilsson, J., Paolo, F. S., et al. (2020). Pervasive ice sheet mass loss reflects competing ocean and atmosphere processes. *Science*, *368*(6496), 1239–1242.Smith, B., S. Dickinson, B. P. Jelley, T. A. Neumann, D. Hancock, J. Lee, & K. Harbeck. (2021). ATLAS/ICESat-2 L3B Annual Land Ice Height, version 4 [Data set]. NASA National Snow and Ice Data Center DAAC. https://doi.org/10.5067/ATLAS/ATL11.004Spikes, V. B., Hamilton, G. S., Arcone, S. A., Kaspari, S., & Mayewski, P. A. (2004). Variability in accumulation rates from GPR profiling on the West Antarctic plateau. *Annals of Glaciology*, *39*, 238–244.Studinger, M., Medley, B. C., Brunt, K. M., Casey, K. A., Kurtz, N. T., Manizade, S. S., et al. (2020). Temporal and spatial variability in surface roughness and accumulation rate around 88° S from repeat airborne geophysical surveys. *The Cryosphere*, *14*(10), 3287–3308.Van Wessem, J. M., Jan Van De Berg, W., Noël, B. P., Van Meijgaard, E., Amory, C., Birnbaum, G., et al. (2018). Modelling the climate and surface mass balance of polar ice sheets using racmo2: Part 2: Antarctica (1979-2016). *Cryosphere*, *12*(4), 1479–1498.